SAR data and field surveys combination to update rainfall-induced shallow landslides inventory

Pietro Miele[a], Mariano Di Napoli[b*], Alessandro Novellino[c], Domenico Calcaterra[a], Jordi J. Mallorqui[d], Diego Di Martire[a,e]

[a] *Department of Earth, Environment and Resources Sciences, Federico II University of Naples, Complesso Universitario di Monte Sant'Angelo, Via Cinthia, 21 – 80126, Naples, Italy*

[b] *Department of Earth, Environmental and Life Sciences, University of Genoa, Corso Europa, 26 – 16132, Genoa, Italy*

[c] *British Geological Survey, Keyworth, NG12 5GG, Nottingham, UK*

[d] *CommSensLab-Universitat Politècnica de Catalunya, D3-Campus Nord-UPC, C. Jordi Girona 1-3, 08034, Barcelona, Spain*

[e] *Sintema Engineering srl – Spin-Off of the University of Naples Federico II, Via Toledo 156, 80134, Naples, Italy*

Corresponding author: mariano.dinapoli@edu.unige.it

Abstract

The *Campania* region has been recurrently hit by severe landslides in volcanoclastic deposits. The city of Naples, and in particular the *Camaldoli* and *Agnano* hills, also suffered several landslide crises in weathered volcanoclastic rocks as a consequence of intense rainfalls or wildfires. This work provides an updated landslide database for the suburbs of Naples. The obtained database consists of about 1322 landslides considering available information dated back to 1816, identified thanks to the historical newspaper's examination; 62 landslides were recorded between 2019 and 2020.

Furthermore, the achieved database is the result of the standardization of available information from different sources, organized in a completely different way. The newly identified phenomena have been recognized thanks to a combination of optical satellite imagery with Google Earth, Sentinel-1 radar satellite imagery and field investigation. The implemented methodology is based on change detection analysis of satellite imagery by using polarimetric features. Subsequently, output derived from the segmentation procedure of satellite images have been compared with field trip observations. The main purpose of this procedure is to emphasize areas where land cover changes, potentially related to slope failures, occur in the Phegraean Fields, facilitating the following possible phases of mapping and/or field survey. Eventually, this type of information is expected to help decision-makers with land planning and risk assessment.

Keywords: amplitude imagery, synthetic aperture radar, landslide, rainfall, Naples

1. Introduction

The request for additional spaces in expanding cities and villages, driven by the continuous population increase, has led to deforestation and cut slopes (Altan et al. 2015; Gariano and Guzzetti 2016). These processes inevitably increase the incidence of landslides, by altering hydrological processes and shear-stress distribution (Wilkinson et al. 2002; Crosta and Frattini 2008). Landslide events globally result in tens of billions of US$ worth of damage and > 4300 lives lost annually (Froude and Petley, 2018). In Europe, and principally in Italy, slope failures represent the main cause of death produced by natural hazards (Guzzetti et al. 2012; Reichenbach et al. 2018). Only in 2019, 3 deaths and 27 injured have been reported and approximately 3,000 people evacuated or remained homeless while, from 1969 to 2020, about 1,100 deaths, 1,500 injured people and thousands of additional evacuees and homeless people have been recorded (https://polaris.irpi.cnr.it/report/last-report/).

Different studies have demonstrated the importance of available up-to-date and complete risk maps, which are based on landslide inventory maps, reducing the impact of these phenomena on society

(Guzzetti et al. 2012). To this respect, it is noteworthy to mention that Italy is one of the very few countries in the world entirely coveded with landslide susceptibility and risk maps since the beginning of the present century. Therefore, there is an urgent need to develop better tools for improving landslide risk management starting from the identification and mapping of landslides reported in the Landslide Inventory Maps (LIMs). The latter provides a detailed picture of landslides within an area by reporting location and, if known, date of occurrence and types of mass movements (Fell et al. 2008; Corominas et al. 2014). LIMs are basic elements in land-use planning and represent powerfully and easily understandable tools for researchers and authorities involved in landslide susceptibility analyses (Lombardo et al. 2015; Segoni et al. 2018; Di Napoli et al. 2020a, 2021; Miele et al. 2021; Arabameri et al. 2021; Yin et al. 2021; Novellino et al. 2021) and landslide risk management (Dai et al. 2002; van Westen et al. 2006; Zhang et al. 2020). Regularly updating LIMs is a strategic activity for territorial planning, also considering that landslides can reactivate over time, even after long periods of quiescence (Guzzetti et al. 2012; Solari et al. 2020).

Over the last three decades, Remote Sensing (RS) technologies based on satellite optical and Synthetic Aperture Radar (SAR(Franceschetti et al. 1992) imagery have been used for landslides detection and mapping (Stumpf et al. 2017; Novellino et al. 2017; Del Soldato et al. 2018; Guerriero et al. 2019). Differently from optical images, SAR data gather ground surface information regardless of weather and illumination conditions. Geoscientists have widely exploited Interferometric SAR (InSAR(Gabriel et al. 1989) techniques to resolve the spatial distribution and temporal evolution of ground instabilities by considering ~~the~~ phase values associated to SAR scenes (Novellino et al. 2015; Confuorto et al. 2017; Raspini et al. 2017; Spinetti et al. 2019). However, due to the inherent limitations of current space observation systems and data processing techniques (Colesanti and Wasowski 2006; Wasowski and Bovenga 2014), InSAR approaches are currently applicable only to extremely slow (<16mm/yr) and very-slow movements (≥1.6mm/yr and ≤16mm/yr) landslides (Cruden and Varnes 1996) which typically correspond to deep-seated gravitational slope deformations, creep, and, in some cases, slides and complex landslides (Saroli et al. 2005; Di Martire et al. 2016; Bozzano et al. 2017).

To overcome such limitations and map ~~rapid~~ deformations induced by relatively rapid landslides, the analysis of amplitude signal associated with the SAR images can be an effective alternative (Mondini et al. 2019). Amplitude-based methods analyse the changes across two images (pre-and post-event) induced by landslide. Despite changes in SAR amplitude have been already used to monitor land cover (Freitas et al. 2008; Qi et al. 2012), many studies have demonstrated the valuable contribution of this approach to detect landslides (Mondini et al. 2017). Still fewer are applications of polarimetric SAR based on amplitude information data for landslides mapping which are limited to large landslides, > km^2 (Shimada et al. 2014; Plank et al. 2016). Polarimetric datasets have been already used in the detection of huge landslides (thousands of square meters) extent: the application here described is aimed to explore the possibility of using amplitude-based methods to recognize landslides with limited extension (hundreds of square meters).

This work aims at the detection of rapid-moving landslides occurred in the *Agnano* plain and *Camaldoli* hill at the end of 2019, both located within the city of Naples (*Campania* region, southern Italy, Figure 1). These sites provide 46% of the whole landslides mapped in the Naples municipality. A semi-automatic procedure aimed to support the detection of rapid-moving landslides from SAR imagery is presented in the following. In most events, ~~the~~ landslides were triggered by high-intensity and short-duration precipitations or prolonged rainfalls affecting the most superficial loose pyroclastic deposits. Furthermore, a rainfall study has been conducted to identify the time span in which landslides could have been detached.

The paper is organized as follows: first, the geological and geomorphological setting of Naples' municipality area is presented along with a brief characterization of rainfall events which occurred in the examined area during the considered period. The data and methods used in the work are successively analysed. Further, an overview of basic concepts of the polarimetric SAR amplitude technique is described. Finally, polarimetric outcomes are compared with field surveys data to evaluate the applicability of the semi-automatic procedure to landslide detection.

2. Materials and Method

2.1 Study area

The *Agnano* plain and *Camaldoli* hill are located in the eastern sector of the Phlegraean Fields, an active volcanic field of ~ 450km^2 in size located west of the city of Naples. The area has experienced numerous eruptions from monogenic volcanoes over the past 70,000 years (Scarpati et al. 2013, 2015); (Figure 1) but local landscape and bedrock geology is mainly characterized by two eruptions: Campanian Ignimbrite eruption (CI - occurred 39,000 years; Rolandi et al., 2020) and the Neapolitan Yellow Tuff eruption (NYT- occurred 15,000 years ago; Scarpati et al., 2013). These sequences are covered by pyroclastic, anthropogenic, and epiclastic deposits with abrupt variations in thickness and facies that are very susceptible to landslides.

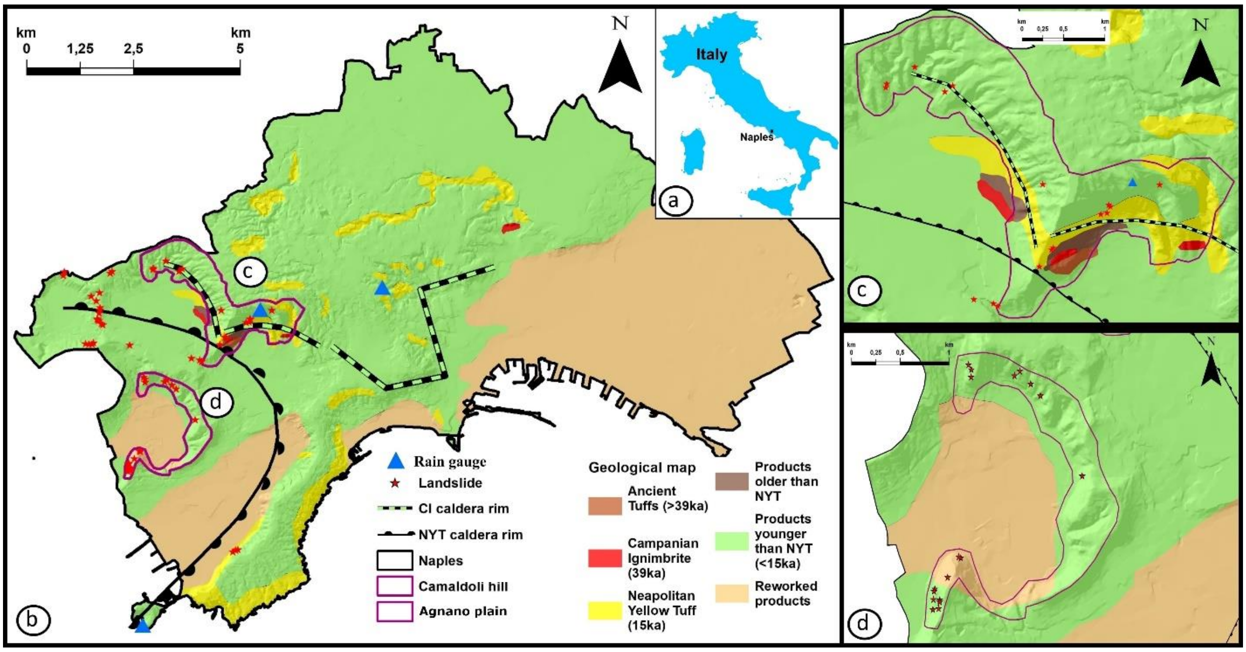

Figure 1. a) Location of the study area; b) geological sketch map of the urban area of Naples (modified from Scarpati et al. 2015); c) and d) detailed view of *Camaldoli* hill and *Agnano* plain, respectively (western sector of city of Naples, purple bold line in a).

The morphology of the whole Phlegraean area reflects the evidence of volcano-tectonic Quaternary events and the slopes are the remains of ancient volcanic buildings. These hills consist of several tens of metre thick NYT and are generally covered by younger (< 15 ka) loose and unconsolidated pyroclastic deposits (Ascione et al. 2020). Additionally, the energy of relief is quite high where local hills are characterized by high slope angles (> 30°). The caldera inner slopes have typical semi-circular planar shapes and steep profiles that make them prone to landsliding (Calcaterra et al. 2007; Ascione et al. 2020). Also, the drainage network presents a pronounced structural control, where low-order straight channels are exposed (Di Martire et al. 2012). Sea level variations also greatly contributed to the present morphological setting. These conditions have represented predisposing factors for the development of landslides since the Roman era (Morra et al. 2010).

Landslides are the main geomorphic processes within Naples municipality. Although landslides have generated disruption and damage over time, only in recent decades more attention has been posed to these phenomena, following the February 1986 rainfall event, representing a threshold between historical and recent mass movements (Beneduce et al. 1988; Calcaterra et al. 2002; Di Martire et al. 2012) which led to complete landslide inventory in the Phlegraean area (Carratù et al. 2015; Finicelli et al. 2016). The inventories reveal that landslides mostly affect the shallow pyroclastic cover and have thicknesses in the order of 0.5 to 2 m (Calcaterra et al. 2007) and are characterized by relatively low mobility.

2.2 Rainfall analysis and landslide inventory

The intensity of 2019-2020 rainfall phenomena striking the Phlegraean Fields has been compared with historical data available from the Multi-hazard Functional Center of the Campanian Regional Agency for the Environmental Protection, and refer to rain gauges located at the *Camaldoli*, *Pozzuoli* and *Capodimonte* sites (Figure 1b). Considering the geological and geomorphological setting of the Phlegraean Field, rainfall is the main triggering factor of mass movements and can be divided, according to De Luca et al. (2010): 1) frontal rainfall, 2) hurricane-like rainfall, and 3) isolated convective storms. Between September and December 2019, the *Campania* region was affected by several rainfall events of high intensity and, frequently, also short duration.

One of the major events occurred on 26 September 2019, which was characterized by very intense and short-duration rainfall. Rain gauges located in the study area recorded average values of 29.4 mm in 10 minutes followed by 49.6 mm, 61.2 mm and 66.2 of cumulative rainfall in the next 20, 30 and 40 minutes, respectively, values close to the historical maxima observed in the area (Figure 2).

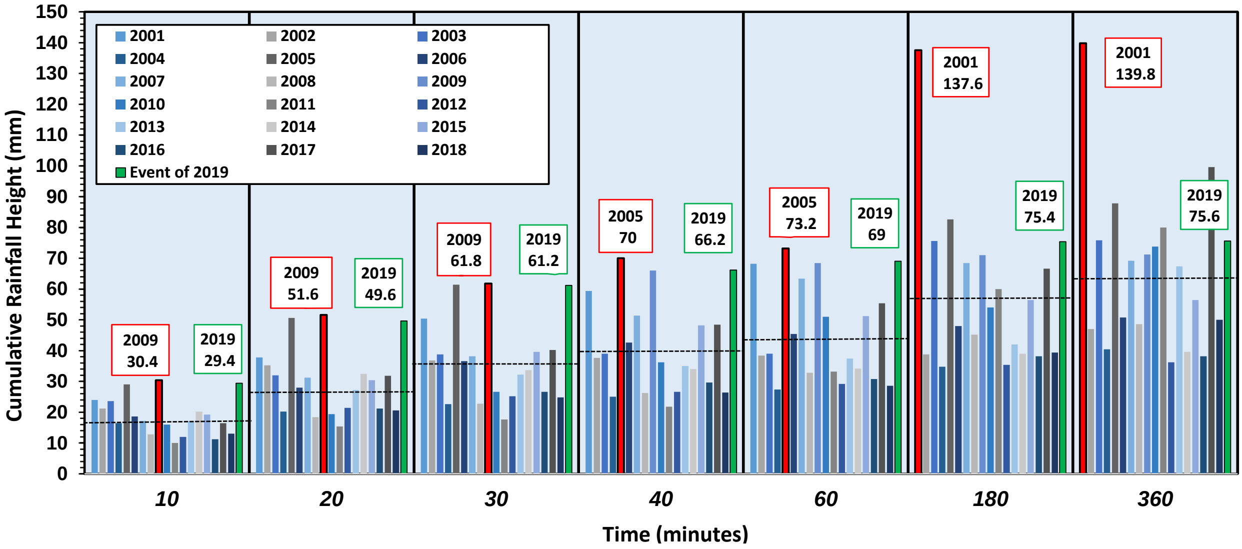

Figure 2. Time series of the maximum daily cumulative rainfall at intervals from 10' to 6h from 2001 to 2019. Red bars highlight the historical maximum rainfall of the study area, while green bars represent rainfall measured in the September 2019 event. Dotted black line indicates the average value for the considered range on the time axis.

Historical data reveal that the Phlegraean district has been already struck by significant short durations of rainfall events in September. For example, in September 2001 there were rainfall events, with an estimated periodicity exceeding 100 years, with high intensity (especially in the first 3 hours). Since 2001 also, other events are characterised by high-intensity and short-duration rainfall (September 2005, June 2009 - http://centrofunzionale.regione.campania.it). In addition, reports on hydrological events by the Multi-hazard Functional Center website show that one of the events that occurred in the examined time span, i.e. 26 September, is characterised by wide return period. An analysis of the rainfall event uniqueness, with the estimation of return period, was carried out based on the Gumbel probability distribution (http://centrofunzionale.regione.campania.it/#/pages/documenti/rapporti). Table 1 shows the values of the return period for maximum rainfall of 10' to 6h duration.

Table 1. Return period for rainfall of the given height

Duration	**10’**	**20’**	**30’**	**60’**	**180’**	**360’**
h (mm)	29.4	49.6	61.2	69.0	75.4	75.6
T (years)	18	25	28	11	5	4

After these events, additional landslides occurred in the study area as a consequence of other high-intensity and short-duration rainfall. Hence, different change detections have been accomplished to identify the number of landslides associated with the different rainfall events and to create a multi-temporal catalogue of the mass movements triggered in the study area.

Several studies have already compiled a partial census of landslide phenomena (Calcaterra et al. 2002; Di Martire et al. 2012; Carratù et al. 2015; Finicelli et al. 2016) in addition to the *I.F.F.I.* (Landslide Inventory in Italy) national landslides database. Despite a large amount of information available, either these sources do not have a common standard for the landslides classification or have the same level of completeness and detail, resulting in a constraint. To overcome these limitations, exploring the different available datasets from historical archives of local newspapers and fire brigade interventions, further phenomena not previously included have been added. Hence, the final database created details a comprehensive catalogue of all the events and, for each of them, provides the following information: date of occurence, landslide detachment location, type of material involved, type of landslide according to Cruden and Varnes (1996), possible triggering mechanism, any damage victim, and the relative source.

Visual interpretation of Google Earth images integrated by geomorphological field survey observations were performed to validate and update the landslide inventory with the latest mass movements that occurred in the area. Field surveys were carried out on topographical maps at 1:5,000 scale between December 2019 and February 2020, following the intense rainfall phenomena that occurred in the Phlegraean area. Based on the scale adopted in mapping activity, only landslides larger than 25 m^2 were considered.

2.3 Methodology

The procedure for the individuation and validation of landslides consists of two independent steps. The first part includes the identification of slope failures through field surveys and the creation of a landslide inventory, while the second part is characterized by the collection and processing of radar polarimetric satellite images for the development of another landslide inventory. Finally, the two outputs have been compared to assess the results (Figure 3).

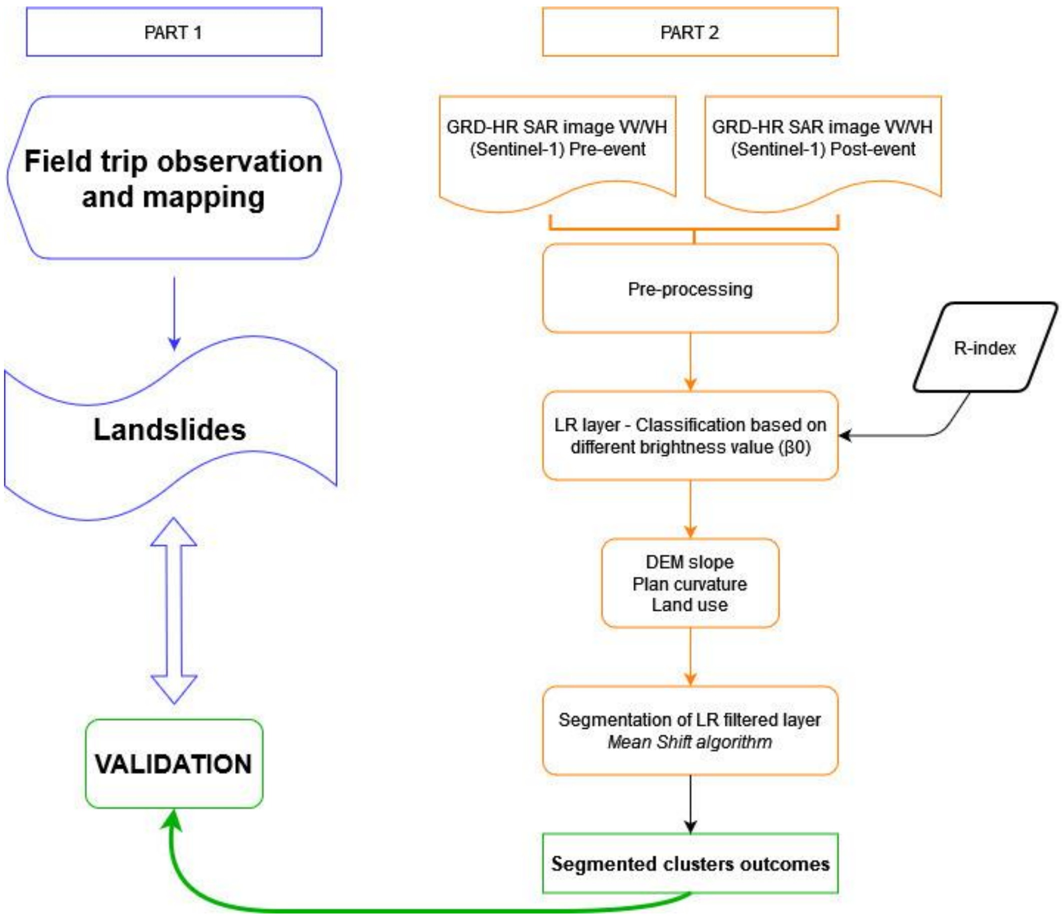

Figure 3. Flowchart of the proposed methodology.

2.3.1 Pre-processing of SAR image

The pre-processing procedure is based on Sentinel-1 images acquired in the Level-1 Ground Range Detected – High Resolution format (GRD-HR) and Interferometric Wide acquisition mode in VV and

VH polarization (https://scihub.copernicus.eu/). Level-1 GRD products are focused SAR data that has been multi-looked and projected to ground range using the Earth ellipsoid model WGS84. Only the amplitude information associated with each pixel in the image was considered (https://sentinel.esa.int/web/sentinel/missions/sentinel-1/data-products). The resulting product has squared pixels of 10 m resolution with reduced speckle.

For the purpose of this work, six images were acquired shortly after the heaviest rainfall recorded in the area, both in ascending and descending orbit and covering the period between 17 September 2019 and 16 January 2020 (Table 2).

Table 2. Analysed SAR imagery in the amplitude change detection. The listed products correspond only to images acquired in descending orbit. The whole considered imagery dataset corresponds to GRD-HR dual-pol products.

Date	Satellite platform
17 September 2019	Sentinel-1B
5 October 2019	Sentinel-1A
5 November 2019	Sentinel-1B
4 December 2019	Sentinel-1A
29 December 2019	Sentinel-1A
16 January 2020	Sentinel-1A

Pre-processing of the images is performed to obtain Beta Nought (β_0), namely the radar brightness coefficient in slant coordinates. This step is done using the open-source software SNAP, available from the European Space Agency, and includes: retrieving the precise orbits, removing the thermal noise and radiometric calibration (Filipponi 2019). SAR images were co-registered with a 10 m Digital Elevation Model (DEM)-assisted procedure (Tarquini et al. 2007). After the co-registration, the resulting stacked images are filtered for speckling reduction using the adaptive Frost filter (Frost et al. 1982), with a filter size in X and Y of 5 pixels, and a damping factor of 2.

2.3.2 Visibility maps

SAR images are very useful tools for detecting and monitoring land cover changes but, being sensed in a side-looking configuration (Kropatsch and Strobl 1990), it is important to predict if the measurements over the study area might be affected by geometrical distortions before any processing. A preliminary analysis was carried out to obtain the Range Index (RI) (Notti et al. 2012, 2014), the latter is a pixel-by-pixel representation of the relationship between the geometry of acquisition of the satellite (slant range) and the topography (Slope angle (S) and slope Aspect (A); (Plank et al. 2012; Del Soldato et al. 2021). The elements needed to calculate the RI are a DEM and the satellite Line of Sight (LoS) parameters, namely the incidence angle (α) and heading (θ). The maximum value of RI is 1. This occurs when the slope is parallel to the LoS. This is the best geometry to detect PS in mountainous areas. On the contrary, the lowest value of RI occurs in the case of foreshortening ($0 < RI < 0.3$) or layovering ($RI < 0$) effects. Obtained outcomes have been classified according to the four main RI classes suggested by Notti et al. (2012).

2.4 SAR amplitude changes detection

Analysing changes between pre-and post-event amplitude SAR images is based on the assumption that landslides change the local land cover and its properties. When mass movements occur, if the mobilised material covering the previous surface is characterized by a higher moisture content then the backscatter signal should drop (Novellino et al. 2020). On the contrary, the increase in the backscatter signal means that new and dry outcrops might have been uncovered. Back-scattering might also increase when the surface roughness (at the scale of the used wavelength) increases (Oliver and Quegan 2004) for example as a result of trees being ripped off leaving bare soil or rock. Such changes are similar to the ones induced by rapid-moving landslides. Following the procedure defined by (Mondini 2017), the Log-Ratio (LR) index was then computed in every pixel for each couple of dual-pol consecutive images. LR index estimates change in brightness that can be induced by land cover changes due to both natural (e.g., landslides, floods, snow melting) or human-induced activities (e.g., deforestation, mining activities) in a defined time interval. The obtained ratio image helps suppressing background structures and improve the detectability of potential changes from SAR data (Ajadi et al., 2016).

For each pair of corresponding pixels belonging to consecutive pre-processed SAR images, LR is calculated as follows (Esposito et al. 2020) (Eq. 1):

$$LR = \ln\left(\frac{\beta_{0,i}}{\beta_{0,i-1}}\right) \qquad \text{(Eq. 1)}$$

where β_0 is the reflectivity per unit area in slant range; its values are independent from the terrain covered and *i* indicate two consecutive pre-processed SAR images. LR pixels can be signed by positive or negative values, depending on the backscattering changes. Then, a subset of Region of Interest (RoI) is extracted by using the subset tool in SNAP.

2.5 Image segmentation and matching assessment

LR layer segmentation groups pixels with similar LR values into various unique segments. The image is partitioned into regions that contain points having nearly the same properties, e.g. mean values or textural properties (Tang 2010). In this work, segmentation process is performed with the "*i.segment*" module in GRASS GIS 7.8.3 using the "Mean Shift" algorithm and the adaptive bandwidth option (Fukunaga and Hostetler 1975). Before the segmentation, a filtering step has been performed to mask pixels that, cannot correspond to landslides (i.e., flat and urban areas). In fact, to obtain an LR filtered layer, areas potentially affected by mass movements were separated using morphological parameters derived from slope and plan curvature. Additionally, areas in shadowing and foreshortening in the RI have been masked out and removed. Moreover, to ensure the correct identification of urban boundaries, land-use information derived from the second level of the 2018 Corine Land Cover (CLC) program were taken into account (https://land.copernicus.eu/pan-european/corine-land-cover/clc2018). CLC classification system is hierarchical and subdivided into different levels:, the second level of the CLC classification for the urban group includes areas mainly occupied by dwellings and buildings used by administrative/public utilities, including their connected areas (associated lands, approach road network, parking lots).

To obtain pixel groups with similar LR values, segmentation of the LR filtered layer is carried out. For this purpose, the algorithm requires the definition of the following parameters: *i*) a selective threshold with a value between 0 and 1; *ii*) the kernel size; *iii*) the minimum number of cells falling into a cluster and *iv*) the minimum number of iterations. A threshold of 0 would allow only pixels with identical values to be considered similar and clustered together in a segment, while a threshold of 1 would allow everything to be included in a large segment (Momsen and Metz 2017). Mean Shift algorithm recalculates central pixel values using the user-defined maximum number of iterations or until the shift between the central pixel and pixels within the kernel results is smaller than the user-defined threshold. The threshold choice depends on the purpose of the application and the image resolution (Comaniciu and Meer 1999; Tao et al. 2007). To select the appropriate parameter values, iterative steps have been carried out manually. According to (Esposito et al. 2020), the criterion for selecting the best input values is to search for the combination of values that optimize, at the same time, the number of clusters and their average size concerning the expected land cover changes. In this work, to avoid over-segmentation a threshold value of 0.1 and a minimum of 3 pixels to determine the presence of a cluster with the Euclidean calculation method have been chosen. Considering the approximate expected size of the land cover changes, the size of the spatial kernel was set to 10 pixels with 200 iterations to detect significant differences in LR values and to minimize the "*salt and pepper effect*" both for VH and VV polarization LR layers.

The obtained outcomes have been matched with the surveyed data reported in the LIM map. This procedure allowed to compare the two datasets in terms of landslide number recognized and their areal extension.

3. Results and discussion

3.1 Change detection analyses

The preliminary analysis based on the RI calculation shows that the most of the slopes in the *Agnano* and *Camaldoli* areas is affected by topographic effects limiting SAR applications (Figure 4). The ascending orbit is characterized by a low RI (< 0.3). As shown in Figure 4, the western side of *Camaldoli* slopes and almost all of the *Agnano* slopes fall into a low RI class. By comparing ascending and descending orbits, it is possible to note that the descending geometry is better suited for slopes facing west. On the contrary, the ascending geometry allows to better investigate slopes oriented to East. Considering the western wards landslides' directions of motion, only descending SAR images have been employed in this work.

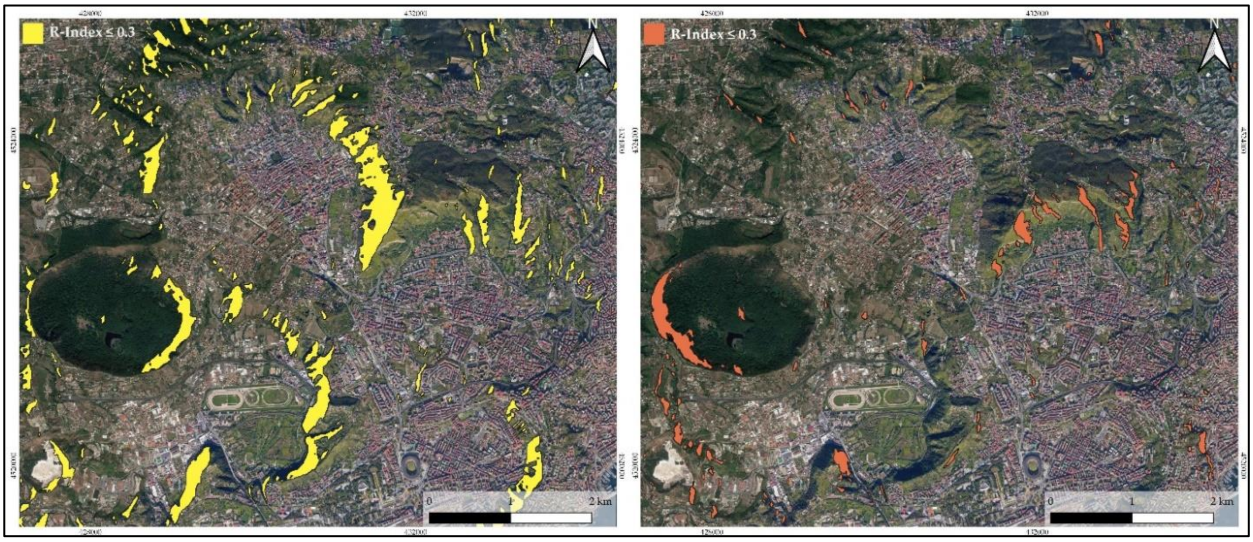

Figure 4. Visibility maps of *Camaldoli* hill and *Agnano* plain in the ascending geometry (left) and descending geometry (right). In ascending geometry most of the slopes are affected by layover and shadowing problems due to the topography effects and LoS parameters.

Subsequently, LR has been filtered out by selecting only flat areas and urban settlements. After the segmentation of the LR filtered layer, segments with a minimum size of 3 pixels, corresponding to a minimum area of 300 m^2, were extracted in the RoI. The output of the segmentation algorithm returned 39 clusters in the *Camaldoli* and *Agnano* areas (Figure 5). The obtained outcomes correspond to small and isolated clusters in a homogeneous region. These outputs have been interpreted taking into account the geometry of the cluster: i.e., clusters running perpendicular to the line of the maximum slope were not considered as well as clusters that cover areas too large are not compatible with the typical landslides historically occurred in the study area. Concerning the multi-temporal analysis, different change detections were analysed considering different images acquired at monthly intervals and the analysis of the daily rainfall during the period studied and making it possible to identify the probable trigger periods of the landslides. Specifically, in the period between September and October two landslides were recorded on the *Camaldoli* hill while four phenomena were identified between October and November in *Agnano*. Between November and December, a total of five landslides were identified in *Agnano* (i.e., 3) and *Camaldoli* (i.e., 2) and finally, the eleven events were mapped between December and January 2020 on the slopes of the *Agnano* plain (Table 3 and Figure 5, see Supplementary Material to consult all performed change detection).

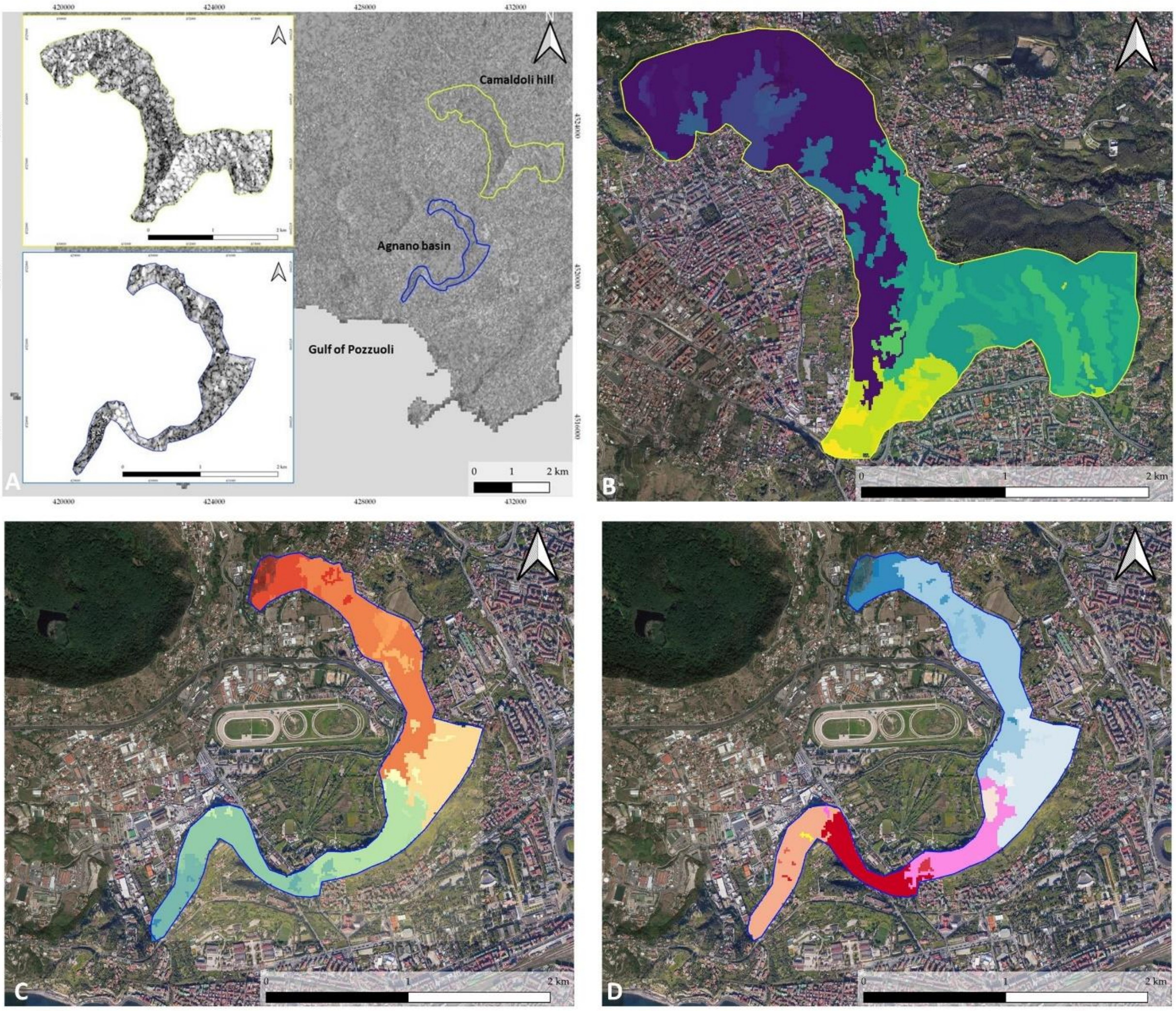

Figure 5. Outputs from the segmentation step: a) LR amplitude layer of the RoI within part of Phlegrean Fields obtained stacking the last two SAR images considered (29 December 2019 and 16 January 2020) clipped around the *Agnano* plain and *Camaldoli* hill areas; b) segmentation results for the October-November period in the *Agnano* area; c) results for the December-January period over the Agnano basin; d) results for December at the Camaldoli hill.

Table 3. Summary of landslides recognition for each change analysis computed.

TIME SPAN	*AGNANO*	*CAMALDOLI*
SEPTEMBER/OCTOBER	-	2
OCTOBER/NOVEMBER	4	-
NOVEMBER/DECEMBER	3	2
DECEMBER/DECEMBER	-	5
DECEMBER/JANUARY	11	-
SUM OF CHANGE DETECTION	18	9

3.2 Landslide inventory

The re-analysis of all the available databases resulted in 1,322 phenomena covering a time span from 1816 to 2020. Regrettably, not all the fields entered are complete and the reasons are manifold:

- first of all, only with the surge of media in recent decades, more attention has been posed towards the reporting of slope movements;
- the growing interference of natural landscapes with anthropic settlements due to the demographic increase and the urbanization which, in turn, has led to a significant increase in the elements at risk;
- furthermore, the Phlegraean phenomena affect the most superficial part of the pyroclastic cover, so promoting the rapid obliteration, through weathering and vegetation re-growth, of landslide geomorphological scars.

Of the 62 additional landslides recognized throughout the area of Naples, 29 mass movements are located on the slopes of the *Agnano* plain and the *Camaldoli* hill so confirming that these areas have the highest susceptibility within Naples (Figure 1b). These mass movements cover a total area of 38,760 m^2. About 50% of the total landslides surveyed fall in the areas mentioned above, with a high density of landslides (*Pianura*/*Soccavo*: 23 landslides/km^2, *Agnano*: 16 landslides/km^2). Slope failure size ranges from a minimum value of 81 m^2 to a maximum one of 1745 m^2 whereas the average area is 635 m^2. Following Cruden and Varnes (1996) and Hungr et al. (2014) classifications, most of the landslides can be classified as rotational or translational slides (26%), which are typical phenomena affecting local hilly areas, particularly in case of prolonged or intense rainfall events. The above-mentioned problems, together with land-use changes (i.e., abandonment of agricultural practices; Figure 6) and wildfires, have caused a progressive increase in landslide occurrence over time. These problems combined with the urban sprawl has increased the landslide risk in this context (Calcaterra et al. 2007; Di Napoli et al. 2020b). The integration between RS and conventional geological methods can represent a significant tool for intervention works planning, providing the right indication on how and where to operate to reduce the risk and to increase the safety of the area.

Figure 6. Interaction between land-use change (green) and landslides (red). Lateral landslides were detached at the base of the terraced areas where the agricultural practices are still active, differently from the central landslide.

Debris flows are not widely distributed (4%); they usually occur simultaneously with flash floods and are characterized by rapid and very rapid surging flows of saturated debris entrained from the flow path and of landsliding materials entered in the channels from the slopes. On the other hand, the tuffs are affected by falls and topples (23%), which move from high-angle walls and, more frequently, from cut slopes or quarry walls (Calcaterra et al. 2002). Finally, many landslides (38%) with complex evolution can be observed along the Phlegrean hilly slopes. These phenomena are characterized by localized residual movements and occasional reactivations. Although rainfall remains a significant trigger (73%), human activities have taken on a clear relevance. These numbers are associated with the data acquired during the study and consultation of the sources for the census of landslides (Figure 7).

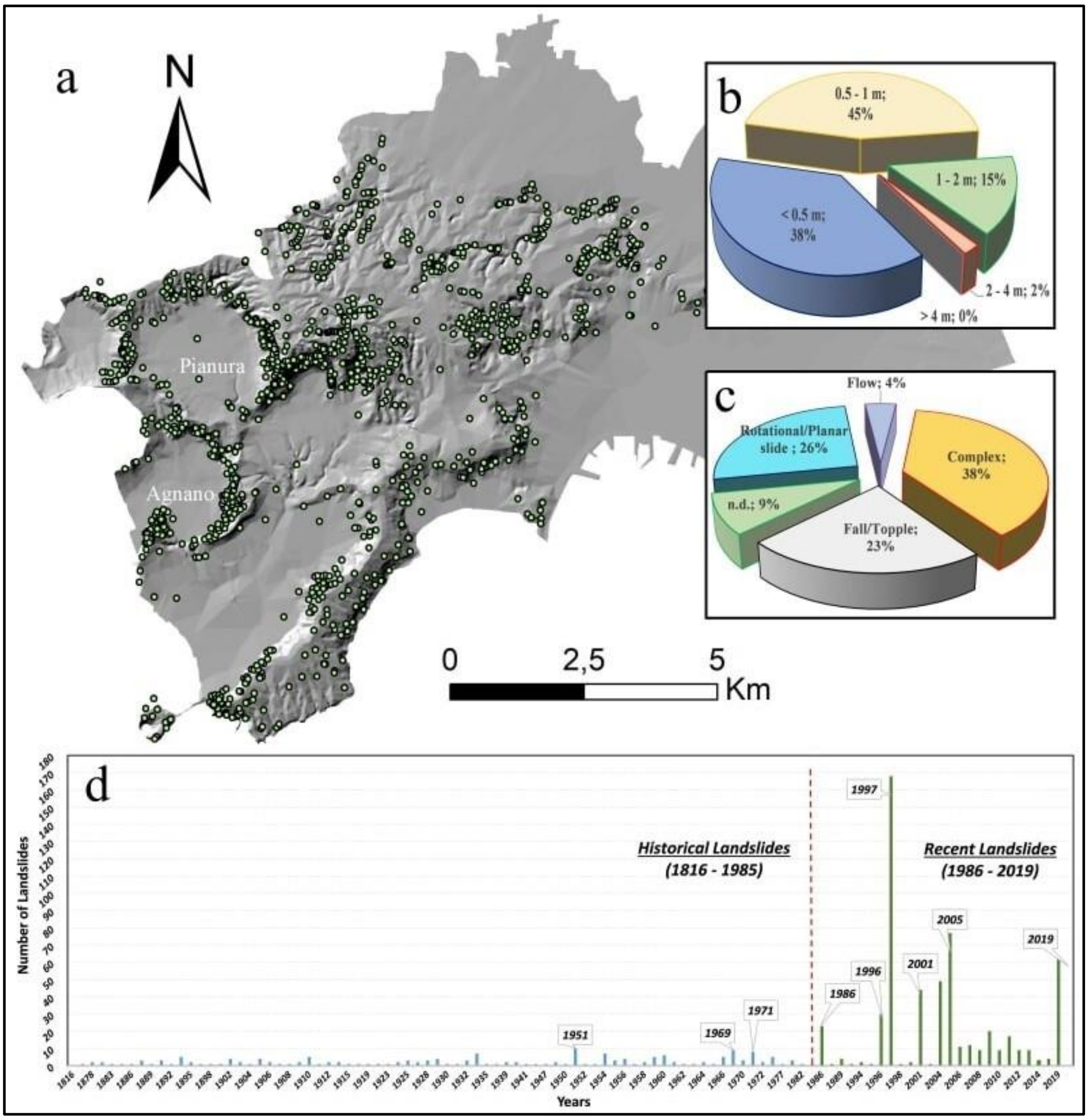

Figure 7. a) Landslide inventory map for the Naples municipality; b) percentage of landslides vs thickness of superficial deposits; c) percentage of landslides by typology; d) annual distribution of landslides in Naples for the period 1816 - 2020. Red line remarks the threshold between "historical" and "recent" landslides.

3.3 SAR and field surveys comparison

Twenty-seven of 39 clusters individuated with the segmentation process correspond to landslides detected in the field. The remaining 12 clusters could be interpreted as false-positive, because small landslides can be immediately obliterated or the amplitude-based method might detect slope failures in areas inaccessible to survey, or false-negative due to limited spatial resolution of the SAR products. True positives correspond to 78.8% and, if landslides >300 m^2 are taken into account, the value increases to 80% (Figure 8). Other landslides surveyed in the field are too small considering the resolution of available radar imagery used. The recognised clusters show an areal extent of landslide slopes larger than the areas recognised during the field survey. This overestimation is unfortunately due to the low satellite images resolution that, when small landslides occur, do not allow the exact delimitation of the landslide area (East sector of *Camaldoli* hill, Figure 8). However, satellite data allows precise identification of landslides location, especially when are present area inaccessible to field detectors, as demonstrated on *Camaldoli* hill.

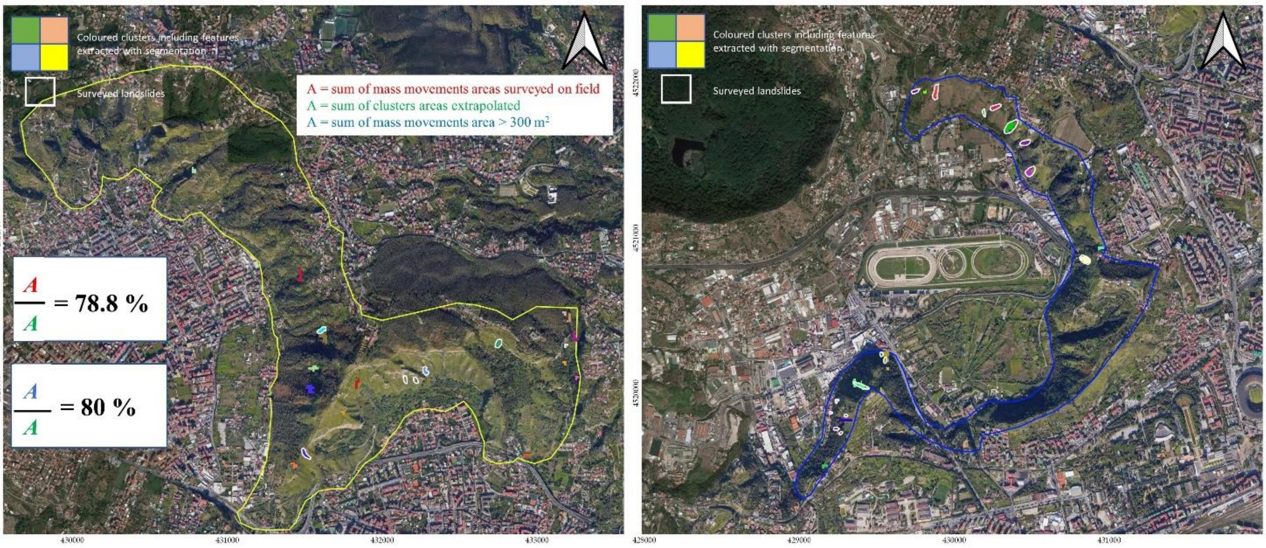

Figure 8. Comparison between the SAR derived segmentation map and the field investigation. In the *Agnano* plain (right) there is a good correspondence between landslides' shapes and clusters. The *Camaldoli* hill area presents many clusters corresponding to false-positive objects due to issues of visibility parameters (see visibility maps).

5. Conclusions

Over the last decades, remote sensing technologies have supported landslide monitoring and detection analyses at relatively low costs. Among them, amplitude-based methods have been employed in very large mass movements identification. A semi-automatic procedure to identify rapid landslide occurrence in measures of SAR amplitude changes has been tested in this work over the hills of Naples (Italy). The scope of our method is to obtain preliminary information from radar imagery on mass movements when atmospheric conditions (cloud coverage) prevent the use of optical images. For the chosen study area, only SAR images acquired in descending orbit were considered due to the geometrical constraints recorded in the ascending orbits. At the same time, extensive field surveys activities have been executed in the study area in order to update the landslide inventory. Moreover, the inventory was re-organized based on all the information available. The results obtained, with 27 events confirmed by field surveys, assert that SAR Sentinel-1 images are successful in capturing rapid landslides. SAR images permit to obtain quick and reliable information in supporting disaster management civil protection operations on landslides occurrence following a rain event when cloud-free optical images are not available. Moreover, in bibliography polarimetric applications have been already presented focusing on very huge mass movements detection. As showed in the results section, thanks to this methodology, it is possible to identify also landslide with limited extension (hundreds of square meters) which are more likely in urban contexts. Further applications could be implemented by using SAR images with very high resolution allowing more accurate results.

Therefore, the proposed methodology may be particularly useful for areas where rainfall-induced shallow landslides represent a threat to human lives, buildings and infrastructures. In particular, this procedure will be helpful for urban and land planning, as well as for decision-makers and stakeholders, to recognize areas where rainfall-induced shallow landslides occur and to identify areas where hazard mitigation measures are required. Hence, this tool represents a step forward for more proper territorial planning and risk response strategy.

Author Contributions: Conceptualization, P.M., M.D.N., D.D.M.; data curation, P.M., M.D.N., A.N.; formal analysis, P.M., M.D.N., A.N.; investigation, M.D.N, D.D.R., D.C.; methodology P.M., D.D.M., A.N.; software P.M., A.N.; validation, M.D.N., D.D.M., D.C.; writing – original draft preparation P.M., M.D.N., A.N.; writing – review and editing, J.M. and D.C.; supervision, D.D.M. all authors have read and agreed to the published version of the manuscript.

Funding: The work was funded by the scholarship "P.O.N. Dottorati innovativi a caratterizzazione industriale 2014-2020" and by the Spanish MICIN, the State Research Agency (AEI) under projects TEC2017-85244-C2-2-P and PID2020-117303GB-C21 MCIN/AEI/10.13039/501100011033.

Data Availability Statement: For consulting the reported results, it's possible to contact Mariano Di Napoli.

Acknowledgments: The authors thank Consorzio interUniversitario per l aprevenzione dei Grandi Rischi (CUGRI) for providing technological support.

Conflicts of Interest: The authors declare no conflicts of interest.

References

Altan O, Alcántara-Ayala I, Baker D, et al (2015) Disaster Risks Research and Assessment to Promote Risk Reduction and Management. Sociology & Anthropology Department Faculty Publications

Arabameri A, Pal SC, Rezaie F, et al (2021) Decision tree based ensemble machine learning approaches for landslide susceptibility mapping. Geocarto International 0:1–35. https://doi.org/10.1080/10106049.2021.1892210

Ascione A, Aucelli PPC, Cinque A, et al (2020) Geomorphology of Naples and the Campi Flegrei: human and natural landscapes in a restless land. Journal of Maps 0:1–11. https://doi.org/10.1080/17445647.2020.1768448

Beneduce P, D'elia G, Guida M (1988) Morfodinamica dei versanti dell'area Flegrea (Campania) : Erosione in massa ed erosione lineare. Memorie della Societa Geologica Italiana 41:949–961

Bozzano F, Mazzanti P, Perissin D, et al (2017) Basin Scale Assessment of Landslides Geomorphological Setting by Advanced InSAR Analysis. Remote Sensing 9:267. https://doi.org/10.3390/rs9030267

Calcaterra D, Coppin D, de Vita S, et al (2007) Slope processes in weathered volcaniclastic deposits within the city of Naples: The Camaldoli Hill case. Geomorphology 87:132–157. https://doi.org/10.1016/j.geomorph.2006.03.040

Calcaterra D, de Riso R, Nave A, Sgambati D (2002) The role of historical information in landslide hazard assessment of urban areas: the case of Naples (Italy). In: Proc. 1st European Conf. on Landslides, Prague, Czech Republic, 24–26 June 2002

Carratù MT, Di Martire D, Finicelli GF, Calcaterra D (2015) Comparison of bivariate and multivariate analyses for landslide susceptibility mapping in the Phlegraean district: the case study of Camaldoli hill (Napoli, Italy). Rend Online Soc Geol It 35:50–53. https://doi.org/doi: 10.3301/ROL.2015.61

Colesanti C, Wasowski J (2006) Investigating landslides with space-borne Synthetic Aperture Radar (SAR) interferometry. Engineering Geology 88:173–199. https://doi.org/10.1016/j.enggeo.2006.09.013

Comaniciu D, Meer P (1999) Mean shift analysis and applications. In: Proceedings of the Seventh IEEE International Conference on Computer Vision. pp 1197–1203 vol.2

Confuorto P, Di Martire D, Centolanza G, et al (2017) Post-failure evolution analysis of a rainfall-triggered landslide by multi-temporal interferometry SAR approaches integrated with geotechnical analysis. Remote Sensing of Environment 188:51–72. https://doi.org/10.1016/j.rse.2016.11.002

Corominas J, van Westen C, Frattini P, et al (2014) Recommendations for the quantitative analysis of landslide risk. Bull Eng Geol Environ 73:209–263. https://doi.org/10.1007/s10064-013-0538-8

Crosta GB, Frattini P (2008) Rainfall-induced landslides and debris flows. Hydrological Processes 22:473–477. https://doi.org/10.1002/hyp.6885

Cruden DM, Varnes DJ (1996) Landslides: Investigation and Mitigation. Chapter 3 - Landslide types and processes. Transportation Research Board Special Report

Dai FC, Lee CF, Ngai YY (2002) Landslide risk assessment and management: an overview. Engineering Geology 64:65–87. https://doi.org/10.1016/S0013-7952(01)00093-X

De Luca C, Furcolo P, Rossi F, et al (2010) Extreme rainfall in the mediterranean. 9

Del Soldato M, Riquelme A, Bianchini S, et al (2018) Multisource data integration to investigate one century of evolution for the Agnone landslide (Molise, southern Italy). Landslides 15:2113–2128. https://doi.org/10.1007/s10346-018-1015-z

Del Soldato M, Solari L, Novellino A, et al (2021) A New Set of Tools for the Generation of InSAR Visibility Maps over Wide Areas. Geosciences 11:229. https://doi.org/10.3390/geosciences11060229

Di Martire D, De Rosa M, Pesce V, et al (2012) Landslide hazard and land management in high-density urban areas of Campania region, Italy. Nat Hazards Earth Syst Sci 12:905–926. https://doi.org/10.5194/nhess-12-905-2012

Di Martire D, Novellino A, Ramondini M, Calcaterra D (2016) A-Differential Synthetic Aperture Radar Interferometry analysis of a Deep Seated Gravitational Slope Deformation occurring at Bisaccia (Italy). Science of The Total Environment 550:556–573. https://doi.org/10.1016/j.scitotenv.2016.01.102

Di Napoli M, Carotenuto F, Cevasco A, et al (2020a) Machine learning ensemble modelling as a tool to improve landslide susceptibility mapping reliability. Landslides. https://doi.org/10.1007/s10346-020-01392-9

Di Napoli M, Di Martire D, Bausilio G, et al (2021) Rainfall-Induced Shallow Landslide Detachment, Transit and Runout Susceptibility Mapping by Integrating Machine Learning Techniques and GIS-Based Approaches. Water 13:488. https://doi.org/10.3390/w13040488

Di Napoli M, Marsiglia P, Di Martire D, et al (2020b) Landslide Susceptibility Assessment of Wildfire Burnt Areas through Earth-Observation Techniques and a Machine Learning-Based Approach. Remote Sensing 12:2505. https://doi.org/10.3390/rs12152505

Esposito G, Marchesini I, Mondini AC, et al (2020) A spaceborne SAR-based procedure to support the detection of landslides. Natural Hazards and Earth System Sciences 20:2379–2395. https://doi.org/10.5194/nhess-20-2379-2020

Fell R, Corominas J, Bonnard C, et al (2008) Guidelines for landslide susceptibility, hazard and risk zoning for land-use planning. Engineering Geology 102:99–111. https://doi.org/10.1016/j.enggeo.2008.03.014

Filipponi F (2019) Exploitation of Sentinel-2 Time Series to Map Burned Areas at the National Level: A Case Study on the 2017 Italy Wildfires. Remote Sensing 11:622. https://doi.org/10.3390/rs11060622

Finicelli GF, Confuorto P, Carratù MT, Martire DD (2016) Multivariate Statistical approach vs. Deterministic physically based model for landslide susceptibility assessment. ROL 41/2016: https://doi.org/10.3301/ROL.2016.116

Franceschetti G, Migliaccio M, Riccio D, Schirinzi G (1992) SARAS - A synthetic aperture radar (SAR) raw signal simulator. IEEE Transactions on Geoscience and Remote Sensing 30:110–123. https://doi.org/10.1109/36.124221

Freitas C da C, Soler L de S, Sant'Anna SJS, et al (2008) Land Use and Land Cover Mapping in the Brazilian Amazon Using Polarimetric Airborne P-Band SAR Data. IEEE Transactions on Geoscience and Remote Sensing 46:2956–2970. https://doi.org/10.1109/TGRS.2008.2000630

Frost VS, Stiles JA, Shanmugan KS, Holtzman JC (1982) A Model for Radar Images and Its Application to Adaptive Digital Filtering of Multiplicative Noise. IEEE Transactions on Pattern Analysis and Machine Intelligence PAMI-4:157–166. https://doi.org/10.1109/TPAMI.1982.4767223

Fukunaga K, Hostetler L (1975) The estimation of the gradient of a density function, with applications in pattern recognition. IEEE Transactions on Information Theory 21:32–40. https://doi.org/10.1109/TIT.1975.1055330

Gabriel AK, Goldstein RM, Zebker HA (1989) Mapping small elevation changes over large areas: Differential radar interferometry. Journal of Geophysical Research: Solid Earth 94:9183–9191. https://doi.org/10.1029/JB094iB07p09183

Gariano SL, Guzzetti F (2016) Landslides in a changing climate. Earth-Science Reviews 162:227–252. https://doi.org/10.1016/j.earscirev.2016.08.011

Guerriero L, Confuorto P, Calcaterra D, et al (2019) PS-driven inventory of town-damaging landslides in the Benevento, Avellino and Salerno Provinces, southern Italy. Journal of Maps 15:619–625. https://doi.org/10.1080/17445647.2019.1651770

Guzzetti F, Mondini AC, Cardinali M, et al (2012) Landslide inventory maps: New tools for an old problem. Earth-Science Reviews 112:42–66. https://doi.org/10.1016/j.earscirev.2012.02.001

Hungr O, Leroucil S, Picarelli L (2014) The Varnes classification of landslide types, an update. Landslides 11:167–194

Kropatsch WG, Strobl D (1990) The generation of SAR layover and shadow maps from digital elevation models. IEEE Transactions on Geoscience and Remote Sensing 28:98–107. https://doi.org/10.1109/36.45752

Lombardo L, Cama M, Conoscenti C, et al (2015) Binary logistic regression versus stochastic gradient boosted decision trees in assessing landslide susceptibility for multiple-occurring landslide events: application to the 2009 storm event in Messina (Sicily, southern Italy). Nat Hazards 79:1621–1648. https://doi.org/10.1007/s11069-015-1915-3

Miele P, Di Napoli M, Guerriero L, et al (2021) Landslide Awareness System (LAwS) to Increase the Resilience and Safety of Transport Infrastructure: The Case Study of Pan-American Highway (Cuenca–Ecuador). Remote Sensing 13:1564. https://doi.org/10.3390/rs13081564

Momsen E, Metz M (2017) i.segment

Mondini AC (2017) Measures of Spatial Autocorrelation Changes in Multitemporal SAR Images for Event Landslides Detection. Remote Sensing 9:554. https://doi.org/10.3390/rs9060554

Mondini AC, Chang K-T, Chiang S-H, et al (2017) Automatic mapping of event landslides at basin scale in Taiwan using a Montecarlo approach and synthetic land cover fingerprints. International Journal of Applied Earth Observation and Geoinformation 63:112–121. https://doi.org/10.1016/j.jag.2017.07.016

Mondini AC, Santangelo M, Rocchetti M, et al (2019) Sentinel-1 SAR Amplitude Imagery for Rapid Landslide Detection. Remote Sensing 11:760. https://doi.org/10.3390/rs11070760

Morra V, Calcaterra D, Cappelletti P, et al (2010) Urban geology: relationships between geological setting and architectural heritage of the Neapolitan area. Journal of the Virtual Explorer 36:. https://doi.org/10.3809/jvirtex.2010.00261

Notti D, Herrera G, Bianchini S, et al (2014) A methodology for improving landslide PSI data analysis. International Journal of Remote Sensing 35:2186–2214. https://doi.org/10.1080/01431161.2014.889864

Notti D, Meisina C, Zucca F, Colombo A (2012) Models To Predict Persistent Scatterers Data Distribution And Their Capacity To Register Movement Along The Slope. 697:90

Novellino A, Cesarano M, Cappelletti P, et al (2021) Slow-moving landslide risk assessment combining Machine Learning and InSAR techniques. CATENA 203:105317. https://doi.org/10.1016/j.catena.2021.105317

Novellino A, Cigna F, Sowter A, et al (2017) Exploitation of the Intermittent SBAS (ISBAS) algorithm with COSMO-SkyMed data for landslide inventory mapping in north-western Sicily, Italy. Geomorphology 280:153–166. https://doi.org/10.1016/j.geomorph.2016.12.009

Novellino A, De Agostini A, Di Martire D, et al (2015) Using Data from Multiple SAR Sensors in Landslide Characterization: Case Studies from Different Geomorphological Contexts in Italy. In: Lollino G, Giordan D, Crosta GB, et al. (eds) Engineering Geology for Society and Territory - Volume 2. Springer International Publishing, Cham, pp 395–398

Novellino A, Mansour M, Wang L (2020) Measuring soil moisture with spaceborne synthetic aperture radar data. http://nora.nerc.ac.uk/id/eprint/528355/. Accessed 5 Oct 2021

Oliver C, Quegan S (2004) Understanding Synthetic Aperture Radar Images. SciTech Publishing

Plank S, Singer J, Minet C, Thuro K (2012) Pre-survey suitability evaluation of the differential synthetic aperture radar interferometry method for landslide monitoring. International Journal of Remote Sensing 33:6623–6637. https://doi.org/10.1080/01431161.2012.693646

Plank S, Twele A, Martinis S (2016) Landslide Mapping in Vegetated Areas Using Change Detection Based on Optical and Polarimetric SAR Data. Remote Sensing 8:307. https://doi.org/10.3390/rs8040307

Qi Z, Yeh AG-O, Li X, Lin Z (2012) A novel algorithm for land use and land cover classification using RADARSAT-2 polarimetric SAR data. Remote Sensing of Environment 118:21–39. https://doi.org/10.1016/j.rse.2011.11.001

Raspini F, Bardi F, Bianchini S, et al (2017) The contribution of satellite SAR-derived displacement measurements in landslide risk management practices. Nat Hazards 86:327–351. https://doi.org/10.1007/s11069-016-2691-4

Reichenbach P, Rossi M, Malamud BD, et al (2018) A review of statistically-based landslide susceptibility models. Earth-Science Reviews 180:60–91. https://doi.org/10.1016/j.earscirev.2018.03.001

Rolandi G, De Natale G, Kilburn RJC, Troise C, Somma R, Di Lascio M, Fedele A, Rolandi R (2020) The 39 ka Campanian Ignimbrite eruption: new data on source area in the Campanian Plain. Vesuvius, Campi Flegrei, and Campanian Volcanism. https://doi.org/10.1016/B978-0-12-816454-9.00008-0

Saroli M, Stramondo S, Moro M, Doumaz F (2005) Movements detection of deep seated gravitational slope deformations by means of InSAR data and photogeological interpretation: northern Sicily case study. Terra Nova 17:35–43. https://doi.org/10.1111/j.1365-3121.2004.00581.x

Scarpati C, Perrotta A, Lepore S, Calvert A (2013) Eruptive history of Neapolitan volcanoes: constraints from 40Ar–39Ar dating. Geological Magazine 150:412–425. https://doi.org/10.1017/S0016756812000854

Scarpati C, Perrotta A, Sparice D (2015) Volcanism in the city of Naples. ROL 33/2015: https://doi.org/10.3301/ROL.2015.21

Segoni S, Tofani V, Rosi A, et al (2018) Combination of Rainfall Thresholds and Susceptibility Maps for Dynamic Landslide Hazard Assessment at Regional Scale. Front Earth Sci 6:. https://doi.org/10.3389/feart.2018.00085

Shimada M, Watanabe M, Kawano N, et al (2014) Detecting Mountainous Landslides by SAR Polarimetry: A Comparative Study Using Pi-SAR-L2 and X-band SARs. Transactions of the Japan Society for Aeronautical and Space Sciences, Aerospace Technology Japan 12:Pn_9-Pn_15. https://doi.org/10.2322/tastj.12.Pn_9

Solari L, Del Soldato M, Raspini F, et al (2020) Review of Satellite Interferometry for Landslide Detection in Italy. Remote Sensing 12:1351. https://doi.org/10.3390/rs12081351

Spinetti C, Bisson M, Tolomei C, et al (2019) Landslide susceptibility mapping by remote sensing and geomorphological data: case studies on the Sorrentina Peninsula (Southern Italy). GIScience & Remote Sensing 56:940–965. https://doi.org/10.1080/15481603.2019.1587891

Stumpf A, Malet J-P, Delacourt C (2017) Correlation of satellite image time-series for the detection and monitoring of slow-moving landslides. Remote Sensing of Environment 189:40–55. https://doi.org/10.1016/j.rse.2016.11.007

Tang J (2010) A color image segmentation algorithm based on region growing. In: 2010 2nd International Conference on Computer Engineering and Technology. pp V6-634-V6-637

Tao W, Jin H, Zhang Y (2007) Color Image Segmentation Based on Mean Shift and Normalized Cuts. IEEE Transactions on Systems, Man, and Cybernetics, Part B (Cybernetics) 37:1382–1389. https://doi.org/10.1109/TSMCB.2007.902249

Tarquini S, Isola I, Favalli M, et al (2007) TINITALY/01: a new Triangular Irregular Network of Italy

van Westen CJ, van Asch TWJ, Soeters R (2006) Landslide hazard and risk zonation—why is it still so difficult? Bull Eng Geol Environ 65:167–184. https://doi.org/10.1007/s10064-005-0023-0

Wasowski J, Bovenga F (2014) Investigating landslides and unstable slopes with satellite Multi Temporal Interferometry: Current issues and future perspectives. Engineering Geology 174:103–138. https://doi.org/10.1016/j.enggeo.2014.03.003

Wilkinson PL, Anderson MG, Lloyd DM (2002) An integrated hydrological model for rain-induced landslide prediction. Earth Surface Processes and Landforms 27:1285–1297. https://doi.org/10.1002/esp.409

Yin G, Luo J, Niu F, et al (2021) Machine learning-based thermokarst landslide susceptibility modeling across the permafrost region on the Qinghai-Tibet Plateau. Landslides 18:2639–2649. https://doi.org/10.1007/s10346-021-01669-7

Zhang Y, Wu W, Qin Y, et al (2020) Mapping Landslide Hazard Risk Using Random Forest Algorithm in Guixi, Jiangxi, China. ISPRS International Journal of Geo-Information 9:695. https://doi.org/10.3390/ijgi9110695